ADVANCING EARTH AND SPACE SCIENCES

Water Resources Research

RESEARCH ARTICLE
10.1029/2026WR044293

Key Points:
- Sediment transport variability in braided rivers mainly result from random alternances between recurrent morphological states
- A Markovian state-dependent model is able to reproduce clustering and persistence of transport fluctuations unlike models without morphology
- Morphological state is the control variable linking channel-network organization to the statistical properties of sediment transport rates

Correspondence to:
C. Gotelli,
clemente.gotelli@epfl.ch

Citation:
Gotelli, C., & Ancey, C. (2026). Morphological state transitions and sediment transport variability in braided rivers. *Water Resources Research*, *62*, e2026WR044293. https://doi.org/10.1029/2026WR044293

Received 2 APR 2026
Accepted 14 AUG 2026

Author Contributions:
Conceptualization: C. Gotelli, C. Ancey
Data curation: C. Gotelli, C. Ancey
Formal analysis: C. Gotelli, C. Ancey
Funding acquisition: C. Ancey
Investigation: C. Gotelli, C. Ancey
Methodology: C. Gotelli, C. Ancey
Project administration: C. Ancey
Resources: C. Ancey
Software: C. Gotelli
Supervision: C. Ancey
Validation: C. Gotelli, C. Ancey
Visualization: C. Gotelli
Writing – original draft: C. Gotelli, C. Ancey
Writing – review & editing: C. Gotelli, C. Ancey

Morphological State Transitions and Sediment Transport Variability in Braided Rivers

C. Gotelli[1] and **C. Ancey**[1]

[1]Environmental Hydraulics Laboratory, École Polytechnique Fédérale de Lausanne, Lausanne, Switzerland

Abstract Sediment transport in braided rivers shows significant temporal variability, characterized by intense bursts of transport rates even under steady-state conditions. These fluctuations are often viewed as the consequence of random variations in the local hydraulic conditions and sediment movement. While such explanations emphasize small-scale processes, they do not account for how larger-scale channel structure may organize these fluctuations. The role of reach-scale channel morphology in controlling sediment transport remains unexplored. Here we show that the temporal variability of sediment transport results from switching between a finite set of recurrent morphological configurations. We used the results of a former long-term (1200-hr) laboratory experiment conducted under constant water discharge and sediment supply, in which 16 morphological states were identified using image processing. The present paper shows that the temporal evolution of these states can be modeled using a discrete-time Markov process. We assume that sediment transport depends on the active state of the channel. The state-dependent transport rates can be simulated using either an empirical probability distribution fitted to the data or a Gamma distribution with parameters dependent on stream power. We introduced a third model that ignores morphological state, and simulates transport rates using the bootstrap technique. We used the three models to generate long time series of transport rates, the ensemble statistics of which were compared with the experimental statistics. The three models perform equally well for predicting the mean transport rate and its variance, but the purely Markovian model is superior for predicting the temporal features of transport rates. These findings indicate that variability in bedload transport rates mainly results from the persistence and succession of a finite set of morphological states.

Plain Language Summary Braided rivers are composed of multiple channels that constantly split and reconnect while transporting sediment downstream. Even when water discharge and sediment supply remain constant, the amount of sediment transported by the river can fluctuate strongly through time. These fluctuations often occur as bursts of transport separated by quieter periods. Understanding the origin of this variability is important for predicting how rivers reshape their channels and carry sediment. We used the results of a former laboratory flume experiment in which we filmed the evolution of a small-scale braided river over nearly 2 months. We identified a limited number of recurrent riverbed configurations. In the present paper, we develop three models that aim at predicting the transport rates at the flume outlet. Comparing the model outcomes, we find that sediment transport variability can be explained by how long the riverbed stays in a given configuration and how often it switches to another. Our results cast a new light on a commonly accepted hypothesis in sediment transport modeling: bedload transport is usually assumed to depend on how water flows locally. Our results, however, suggest that much of the variability in sediment transport rates does not depend on local conditions, but rather on large-scale variations in riverbed geometry, as it conditions the magnitude of sediment transport.

1. Introduction

A longstanding issue in river hydraulics is accurately quantifying sediment transport rates, particularly when the riverbed exhibits bedforms. Even in the absence of bedforms (e.g., for planar-bed conditions), estimating transport rates remains notably challenging. The most common approach assumes a one-to-one relationship between the sediment transport rate q_s and the water discharge Q (or any discharge-related variables such as bottom shear stress), that is, $q_s = f(Q)$. Physically, this implies that local hydraulic conditions control the transport capacity (Wainwright et al., 2015). Since the earliest work on sediment transport (du Boys, 1879), many empirical and semi-empirical formulas have been proposed, reflecting the inherent difficulty of finding a universal bed-load transport equation.

This difficulty arises from several concurrent mechanisms, including nonlocal transport effects (Ancey et al., 2015; Falcini & Garra, 2021; Furbish et al., 2017; Li et al., 2024; Sun et al., 2015), the sensitivity of bedload transport dynamics to flood hydrograph duration, magnitude, and shape (Phillips et al., 2018), fluctuations in particle velocity and activity (i.e., the number of moving particles per unit stream bed area) (Ancey et al., 2008), grain sorting (Kleinhans, 2004), the coexistence of different flow regimes (Bagnold, 1966), and sediment availability (Gomez & Soar, 2025). For instance, Furbish et al. (2012) showed that at low transport rates, sediment flux depends not only on local flow conditions but also on gradients in particle activity. Other studies have reached similar conclusions (Ancey & Heyman, 2014) or highlighted the need to introduce a relaxation length to account for the development of bedforms (Bohorquez & Ancey, 2015; Bohorquez et al., 2025; Charru et al., 2004). Indeed, if the Saint-Venant–Exner equations used for modeling morphodynamic evolution are based on a one-to-one relationship $q_s = f(Q)$, linear stability analysis then predicts a stable bed, which conflicts with observations of laboratory flumes or real-world rivers (Balmforth & Provenzale, 2001; Bohorquez et al., 2019).

The development of bedforms makes the problem of predicting bedload transport rates even more complex. The common approach based on the hypothesis of bedload dependence on local flow conditions cannot account for the loss of a one-to-one relationship $q_s = f(Q)$ observed when bedforms develop. Researchers have sought alternatives to this approach. Instead of viewing bedload as sediment carried by water, they view it as the movement of bedforms. In this way, bedload transport does not depend directly on how much water is flowing, but on how the bed deforms. For instance, Simons et al. (1965) defined sediment transport rate as a function of the speed and volume of dunes. Subsequent work refined this idea by treating bedforms as waves, so that sediment transport rate can be expressed as the convolution product of their migration velocity and their shape (Aberle et al., 2012; Gomez et al., 1989; Guala et al., 2014; Nikora, 1984). The difficulty with this approach is that bedforms do not always evolve smoothly through advection–diffusion processes. Instead, they may evolve irregularly through processes of creation, merging, and destruction (Phillips, 2003; Murray et al., 2014). Such behaviour has been documented, for instance, in laboratory experiments by Dhont and Ancey (2018), where abrupt changes in bed configuration (alternate bars in a long flume) occurred even under steady inflow rates, and caused pulses of bedload transport.

Braided rivers offer another example of the complex link between large-scale bed configuration and sediment transport. In these rivers, the channel network is made of multiple interacting channels separated by mobile bars that migrate, split, and reconnect over time (Ashworth & Ferguson, 1986). As a result, the overall channel pattern changes continuously, even when external conditions remain nearly constant (Ashmore, 1991). These changes affect the pathways followed by water and sediment within the reach and can therefore influence the sediment transport rate measured at the outlet. Long-term laboratory experiments have shown that sediment export from braided beds often exhibits strong temporal fluctuations, including sudden bursts of transport (Ashmore, 1988; Redolfi & Tubino, 2014). This variability is often explained by turbulence or grain-scale randomness, but the structure of the channel network itself may also play a pivotal role (Bizzi et al., 2021; Escauriaza et al., 2023; Stecca & Hicks, 2022). Past research shows that experiments of braided rivers lead to different riverbed shapes over time, even if the initial and boundary conditions are the same, and thus to markedly different bedload transport rates (Warburton & Davies, 1994). Laboratory experiments have also shown how braided-river morphology can evolve over time through channel-belt widening and reorganization (Limaye, 2020). Recent research shows that in these experiments, bed patterns are not completely random structures, but on the contrary, they consist of a few recurring shapes, each associated with a specific way that water and sediment flow through the area (Gotelli & Ancey, 2026 to Water Resources Research). As bed evolution involves phases of slow evolution (called *stasis*) interspersed with sudden reconfigurations of the riverbed's planimetric structure, we can refer to braided rivers as systems of punctuated equilibria. Reconfigurations can be localized or concern the entire studied area, and the duration of each phase varies randomly. The open question is whether the change in the system is completely random or if there is a certain determinism in its evolution.

The present study adopts a reach-scale statistical perspective in which the channel's planimetric morphology is treated as a random state variable driving sediment transport. Our key hypothesis is that for braided rivers, the temporal variability of sediment transport results from stochastic transitions between a finite set of recurrent morphological states, each associated with distinct transport characteristics. As a consequence, bedload transport combines two distinct effects: (a) the persistence and succession of morphological configurations, and (b) the variability of transport within each configuration.

We investigate this hypothesis using data from a long-duration (7 weeks) laboratory experiment in which a braided channel evolved under steady-state conditions (i.e., with constant water discharge and sediment supply at the flume inlet, and constant mean slope). The data set includes both the bed configuration obtained from overhead imagery and the sediment transport rate measured at the flume outlet. For a stationary stochastic process $q_s(t)$, variability is fully characterized by its probability distribution and its autocorrelation function (or equivalently its power spectrum). The objective of this study is therefore to determine whether these statistical properties can be reproduced from morphological state dynamics alone, and to identify the minimum level of physical description required to achieve this.

To this end, we evaluate three alternative models of sediment-transport time series. The first and simplest one is a purely statistical model based on bootstrap resampling of the observed transport record, with no dependence on bed configuration. The second and third models explicitly represent the evolving bed configuration as a stochastic process, and assign sediment transport conditionally on the active configuration. In one case, transport values are drawn from empirical state-conditioned probability distributions, whereas in the other they are computed from a Gamma distribution, the parameters of which depend on a stream-power equation calibrated on the experimental data. By comparing these models, we assess to what extent morphological state dynamics are required to reproduce not only the magnitude of sediment transport, but also its temporal properties (persistence of transport active, alternance of slow and fast-evolving phases).

The remainder of the paper is organized as follows. Section 2 presents the experimental setup and the data set used in the analysis, including the procedures used to extract bed configurations from overhead imagery and to measure sediment transport at the flume outlet. Section 3 describes the identification of recurrent bed configurations and introduces the stochastic representation used to model their temporal evolution. Section 4 presents the three modeling approaches considered to reproduce the sediment-transport time series. Section 5 compares the synthetic and experimental transport records and evaluates the ability of each model to reproduce the statistical properties of sediment transport, including its variability and temporal organization. Finally, Section 6 discusses the implications of these results for the interpretation of sediment transport in braided rivers and presents the main conclusions of the study.

2. Empirical Foundations for a State-Based Transport Model

The modeling framework developed in this paper is based on empirical results presented in a previous study that used the same experimental data set (Gotelli & Ancey, 2026).

In that study, we showed that the apparently continuous evolution of a braided channel under steady state conditions can be described as a sequence of recurrent channel configurations, which we call morphological states. These states differ in their spatial structure, their duration, and the amount of sediment they transport. In the present paper, this empirical organization provides the starting point for developing a predictive model of sediment transport.

The working hypothesis is that variability in sediment transport at the reach scale arises from transitions between morphological states that exhibit distinct sediment-transport characteristics. Each state corresponds to a particular arrangement of the channel network, which influences the amount of sediment transported. If the sequence of states and the transport behavior associated with each state can be described statistically, then it becomes possible to generate synthetic sediment-transport time series that reproduce both the mean transport rate and its temporal variability.

Before introducing the modeling framework, we briefly summarize the experimental data set and the main empirical observations that motivate this approach.

2.1. Experimental Setup

The data used in this study come from a long-duration laboratory experiment carried out in a flume 1 m wide and 3.3 m long with a mobile bed of well-sorted sand with median grain size $d_{50} = 1$ mm. During the experiment, both the water discharge and the sediment feed rate were kept constant. The system therefore evolved under steady external conditions. Despite these steady conditions, the channel did not remain stable. Instead, it continuously reorganized through bar migration, channel splitting, abandonment of active threads, and reactivation of previously inactive pathways.

Water entered the experiment through an upstream basin equipped with a honeycomb outlet, which distributed the flow before it reached the mobile-bed section. Sediment was supplied independently at a constant feed rate. At the downstream end, water and sediment left the flume through a straight supercritical overfall with the same width as the inlet.

Sediment was not recirculated. Image acquisition began after several tens of hours of adjustment, once the sediment flux at the outlet was, on average, close to the imposed inlet feed rate. The analyzed interval therefore represents an approximately sediment-balanced condition at the scale of the experimental reach, while allowing for short-term fluctuations in sediment storage and outlet transport. The observed mismatch between sediment feed and outlet export is therefore interpreted as a residual change in sediment storage within the flume.

The finite length of the flume likely influenced the morphology near the inlet and outlet. Longer braided-river flume experiments commonly place the measurement reach downstream from the inlet or use large basins to reduce entrance effects (Egozi & Ashmore, 2008; Limaye, 2020). In the present experiment, these boundary effects were not removed from the analysis but were held constant throughout the run. The morphological states, transition probabilities, and transport statistics should therefore be interpreted as properties of this bounded experimental reach under constant boundary conditions.

The experiment ran for approximately 1200 hr, during which the channel planform was recorded every minute using overhead imagery. From each image, the wetted area of the channel was extracted as a binary mask describing the spatial distribution of flowing water within the corridor. We dyed the water to enhance its contrast with the sediment bed. Each raw image was first cropped to the flume interior, and the wetted corridor was then detected with a color filter in the Hue Saturation Value (HSV) color space tuned to the dyed water. The resulting binary mask identified water-covered pixels and was downscaled before the morphological-state analysis. Sediment transport rate q_s was measured at the flume outlet using a load-cell system and averaged over the same one-minute interval. As a result, each recorded channel configuration in the image sequence is directly associated with a corresponding sediment transport value.

2.2. Recurrent Morphological States

Analysis of the planform image sequence shows that the system repeatedly visits a limited set of channel configurations.

These configurations were identified using a fully data-driven procedure that measures the similarity between images and groups morphologically similar configurations into clusters.

In brief, each binary water mask was treated as a geometric object. Pairwise morphological dissimilarity was quantified with two complementary measures: a Modified Hausdorff Distance, which captures displacement of water-boundary pixels, and a Dice-based distance, which captures changes in wetted-area overlap (Dubuisson & Jain, 1994). The resulting high-dimensional distance representation was first reduced with Principal Component Analysis, retaining 99% of the variance in 67 components, and was then embedded in a three-dimensional morphospace using Uniform Manifold Approximation and Projection (McInnes et al., 2020). Clusters were identified in this morphospace with HDBSCAN, a density-based clustering algorithm that detects stable dense regions and labels sparse transitional configurations as noise (McInnes & Healy, 2017).

The number of states was therefore not prescribed a priori. It resulted from the selected PCA–UMAP–HDBSCAN configuration, which was chosen after a parameter sweep because it produced compact, well-separated, and physically interpretable clusters. This configuration identified 16 recurrent morphological states, with a noise fraction below 10% and validation scores consistent with distinct clusters.

Representative examples are shown in Figure 1. Together, these states cover the range of channel organizations observed during the experiment. They range from narrow configurations with weak braiding or nearly single-thread channels to wide, multi-thread braided networks that occupy a large fraction of the available corridor.

By assigning each image to one of these states, the continuous record of channel morphology can be converted into a discrete sequence that describes how the system switches between configurations over time. This sequence is shown in Figure 2. The system often remains in the same state for extended periods before reorganizing into another configuration. States that appeared earlier in the experiment may also reappear later.

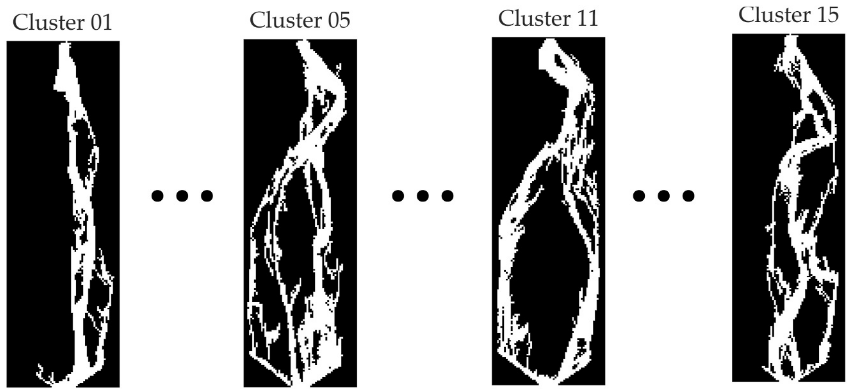

Figure 1. Representative wetted masks for selected morphological states. The states range from narrow, concentrated channel configurations to wide, multi-thread braided networks. In each panel, flow is from upstream at the top to downstream at the bottom.

This discrete representation shows that channel evolution under steady conditions does not occur through smooth and continuous changes. Instead, the system successively visits relatively stable configurations, with fast and abrupt transitions from one configuration to another.

2.3. State-Dependent Sediment Transport

Once channel morphology is described among the recurrent states, sediment transport can be analyzed for each state separately. In practice, this analysis consists of (a) collecting all the transport measurements occurring in a specific state of the system, and then (b) describing the gathered data. This comparison reveals clear and systematic differences between states.

Figure 3 (bottom) illustrates these contrasts. States characterized by a small number of channels, such as State 0 and State 1, tend to show higher median sediment transport rates and wider probability distributions (i.e., strong variability of sediment transport rates). In contrast, wider, multi-thread braided configurations, such as States 9 and 13, generally correspond to lower median transport rates and reduced variability.

This result is supported by earlier studies that found a connection between bedload transport and channel morphology by tracking recurrent morphological states. Note that there are alternative approaches that focus on local morphology (individual bars or channels) or global measures (scalar braiding metrics) to estimate bedload transport rates. It is unclear how these approaches compare or whether one is better than the others (Ashmore, 1988; Redolfi & Tubino, 2014; Warburton & Davies, 1994).

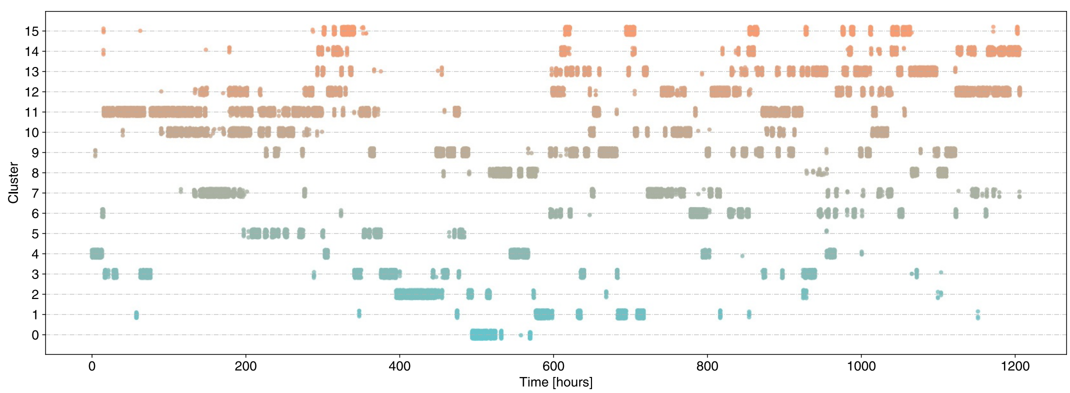

Figure 2. Time series of morphological states during the experiment. Horizontal segments represent periods where the channel remains in the same state, while vertical jumps correspond to rapid reorganization events. States are plotted on separate levels for clarity. Only one state is active at a time.

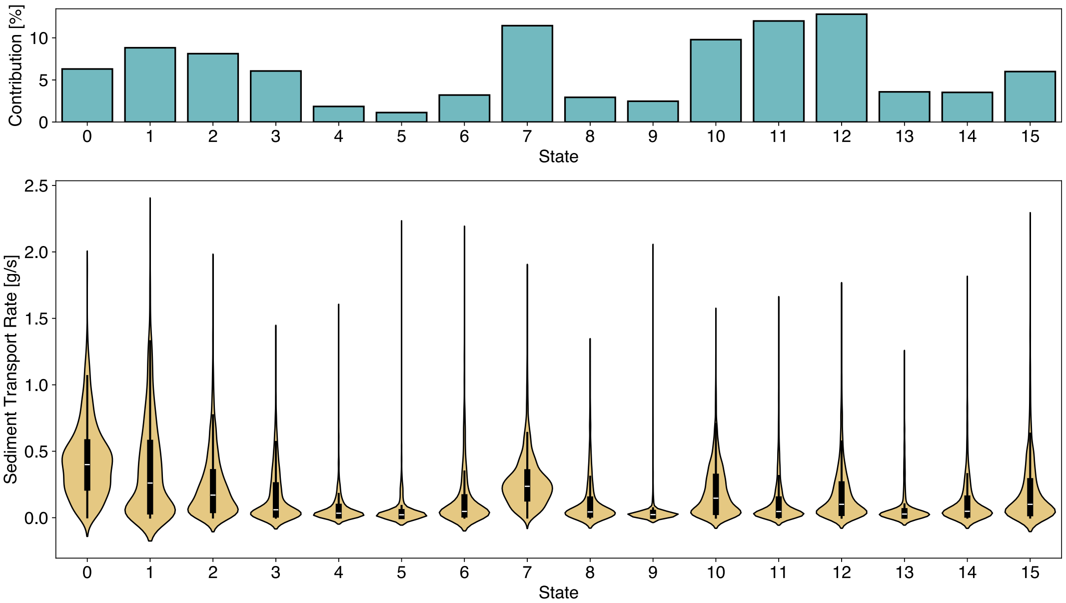

Figure 3. State-conditioned sediment transport. Top: percentage contribution of each state to the total sediment transport. Bottom: empirical probability distributions of sediment transport rate q_s conditioned on state occupancy.

These results show that sediment transport is not statistically stationary. Instead, both the magnitude and the variability of transport depend strongly on the morphological configuration of the channel. In addition, the total sediment export is not evenly distributed across states (Figure 3, top). A limited subset of configurations, such as States 10 to 12, contributes a large fraction of the total transported volume.

2.4. Implications for Modeling

The observations above suggest a simple way to formulate the sediment-transport problem. The transport time series combines two concurrent processes. The first is the temporal evolution of the channel's morphological states. The second is the sediment transport behavior associated with each of these states. As a result, variability in sediment export arises from two sources: fluctuations in transport rates while the system remains in a given state, and transitions between states that have different mean transport rates.

In the following sections, we build on this heuristical formulation by representing the sequence of morphological states as a random process. We then couple this description with transport models defined at the state level. This framework allows us to generate synthetic sediment-transport time series that reproduce the main statistical properties of the experimental record.

3. Probabilistic Representation of Morphological Dynamics

The observations summarized in the previous section indicate that sediment transport variability arises from two distinct processes: the transport behavior associated with each morphological state and the temporal evolution of these states through time. Predicting sediment transport therefore requires not only characterizing the transport properties of individual states, but also describing how the channel visits these individual states.

The experimental image record shows that this evolution is not random. The channel often remains in the same configuration for long periods of time before transitioning into another state. States that appeared earlier in the experiment may also reappear later (see Figure 2). In addition, some transitions occur more frequently than others, and certain states persist much longer. These observations suggest that the sequence of morphological configurations follows a structured albeit random process.

To represent this temporal organization, we seek a probabilistic model capable of generating alternative but statistically consistent histories of morphological evolution under steady conditions. Such a model does not aim to

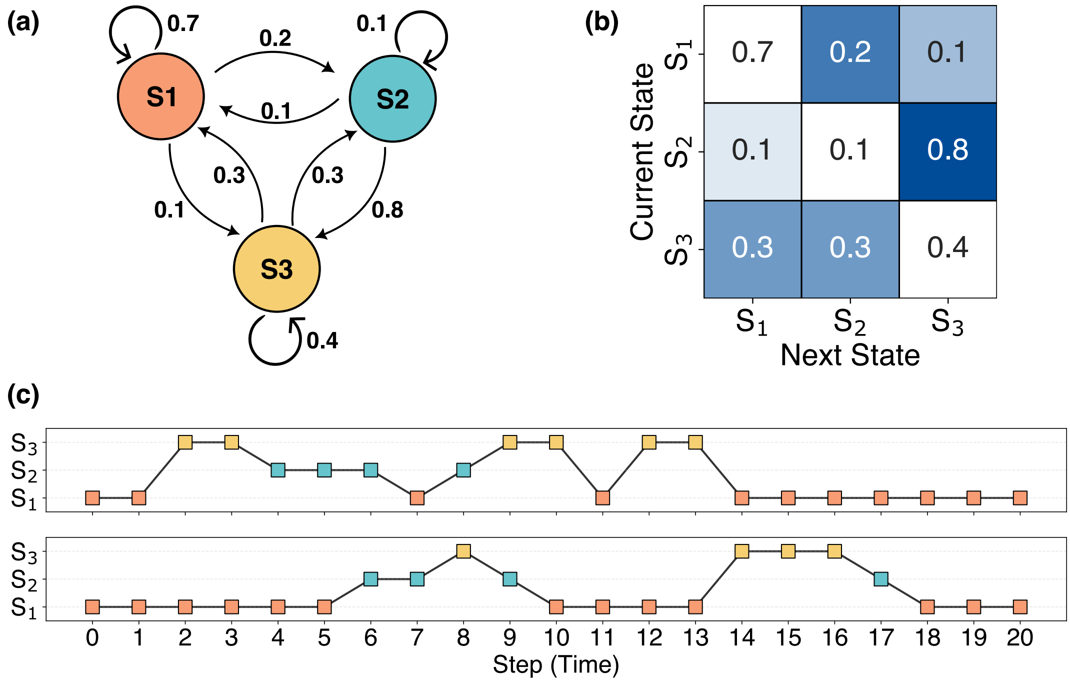

Figure 4. Example of a three-state Markov chain. (a) Transition structure and associated probabilities. (b) Transition matrix summarizing the transition probabilities. (c) Two different realizations generated from the same transition matrix, all starting from S_1.

reproduce the exact sequence observed in the experiment. Instead, it describes the statistical rules that govern how channel configurations follow one another and how long the system tends to remain in a given state.

A natural framework for describing this behavior is a discrete-time Markov chain. In this representation, the system evolves through a finite set of states, and the probability of moving to the next state depends only on the current one (and not on the history of past configurations). The dynamics are described by a transition probability matrix that quantifies how often the system moves from one configuration to another and how long it stays in a given state.

Before applying this model to the 16 morphological states identified in our experiment, we first introduce the concept through a simple illustrative example with three states.

3.1. Three-State Example and Realizations

To illustrate the idea developed in the article, we first consider a toy model with three possible states, denoted S_1, S_2, and S_3. The transition structure and associated probabilities are shown in Figure 4a. For example, if the system is in state S_1, it will remain in S_1 with probability 0.7, move to S_2 with probability 0.2, or move to S_3 with probability 0.1.

These probabilities can be written in the form of a transition matrix P (see Figure 4b), where each row represents the current state and each column represents the next state. The values in each row sum to one because the system must move to one of the available states at the next time step or stays in the same state.

This transition matrix defines the probabilistic evolution of the system. If the system is in state S_i at time t, the state at time $t + 1$ is drawn randomly according to the probability distribution in the i-th row of P. The matrix therefore does not describe a single trajectory but a set of possible paths.

The existence of several possible paths is illustrated in Figure 4c, which shows two different realizations generated from the same transition matrix starting from S_1. Both realizations represent one possible history of the system. Although the trajectories differ in detail, they follow the same transition probabilities and show similar persistence patterns.

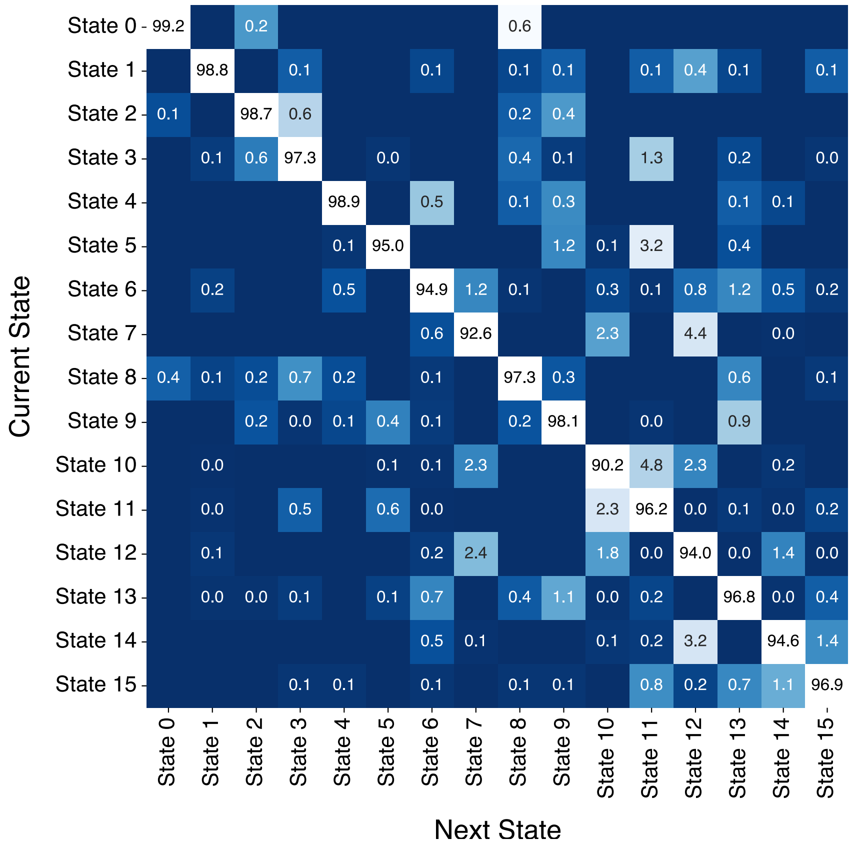

Figure 5. Empirical transition probability matrix for the 16 morphological states. Entry (i, j) gives the probability of moving from state i to state j over one time interval. Lighter colors indicate higher transition probabilities and darker colors indicate lower probabilities. Strong diagonal values indicate persistence, while the off-diagonal structure highlights preferred transitions. Values shown are in percentage.

3.2. Markov Formulation for Morphological States

Let S_t denote the state occupied by the system at time t. The Markov property can then be written as

$$P(S_{t+1} = j | S_t = i, S_{t-1}, S_{t-2}, \ldots) = P(S_{t+1} = j | S_t = i).$$

This condition states that the probability of the next state depends only on the current state. In other words, once the present configuration is known, the system's history does not provide additional information for predicting the next transition. This assumption does not mean that the physical system has no memory. Instead, it assumes that the state at time $t + dt$ depend only on the recent history, so on what happened at time t.

In our experiment, the channel occupies one of 16 morphological states at each observation time. Let $S_t \in \{1, 2, \ldots, 16\}$ denote the state at time step t. The experimental record can therefore be represented as a discrete sequence $S_1, S_2, \ldots, S_T$ describing the temporal evolution of channel morphology under steady conditions (see Figure 2).

The transition probabilities $P_{ij} = P(S_{t+1} = j | S_t = i)$ are estimated directly from the State sequence in Figure 2. This is done by counting how often each transition occurs between consecutive time steps and then normalizing the counts in each row. The resulting empirical transition matrix is shown in Figure 5. The strong diagonal values indicate that states tend to persist for several time steps, while the off-diagonal entries reveal preferred transitions between specific configurations.

By sampling from this transition matrix at each time step, we can generate alternative sequences of morphological states that follow the same statistical transition structure observed in the experiment. These simulated realizations preserve the preferred transition pathways, although the exact timing of transitions may differ from the original record. In the next section, these simulated state sequences are combined with state-level transport descriptions to construct synthetic sediment-transport time series.

4. State-Based Model of Sediment-Transport Time Series

In Section 3, we introduced a probabilistic description of morphological evolution by representing the sequence of states as a Markov process. Building on this representation, we now intend to construct synthetic sediment-transport time series by associating transport values with the state sequences generated by the Markovian model.

We begin with a state-based formulation in which simulated state sequences are coupled with empirical sediment-transport probability distributions conditioned on state occupancy. We then explore a more restrictive formulation in which these empirical probability distributions are replaced by a physically based parameterization derived from stream-power scaling. Finally, we introduce a simple bootstrap model that ignores morphological states entirely and resamples transport values from the full experimental record. This reference model provides a baseline against which the contribution of morphological dynamics can be evaluated.

4.1. Markov Model With Empirical State-Conditioned Sampling

Synthetic sediment-transport time series are generated by combining two elements: (a) simulated sequences of morphological states obtained from the Markov model introduced in Section 3, and (b) the measured sediment-transport values recorded while the system occupied those states (Figure 3). For each morphological state, the experimental data set contains a set of sediment-transport measurements associated with the time intervals during which the channel was classified in that state. These measurements define empirical probability distributions of transport conditioned on state occupancy.

For each step of the simulated state sequence, a transport value is drawn at random (with replacement) from the set of measurements associated with the corresponding state. Repeating this procedure for the entire sequence produces a synthetic time series that preserves both the empirical variability of sediment transport within each state and the probabilistic dynamics of channel morphology.

The construction process of the time series can be illustrated using the three-state example introduced previously. Suppose that sediment-transport measurements have been collected separately for states S_1, S_2, and S_3. These measurements define empirical probability distributions of transport conditioned on state, as illustrated in Figure 6a. Each panel represents the experimental probability distribution of sediment transport while the system occupied the corresponding state.

Consider the first five steps of a realization of the state sequence generated by the Markov chain, such as the example shown in Figure 6b. At each time step t_k the system occupies a particular morphological state. A sediment-transport value is then randomly selected, with replacement, from the set of transport measurements recorded while the channel occupied that state. Repeating this procedure at each time step produces a synthetic sediment-transport time series consistent with the simulated sequence of states.

This time series preserves two key features of the experimental system. First, the ordering and persistence of morphological configurations are governed by the Markov transition matrix, so the temporal clustering of states is maintained. Second, the magnitude and variability of sediment transport associated with each state are drawn directly from the corresponding measured transport values.

The only additional assumption is that transport measurements are independent once the morphological state is specified. Under this assumption, the set of measurements associated with a given state can be regarded as exchangeable samples and resampled with replacement.

In the braided-channel experiment, synthetic state sequences are generated using the empirical transition matrix estimated for the 16 morphological states. Sediment-transport values are then assigned by resampling from the measured transport values associated with each state (see Figure 3). Repeating this procedure produces an ensemble of synthetic sediment-transport time series that reproduce both the persistence of morphological states and the transport variability associated with them.

10.1029/2026WR044293

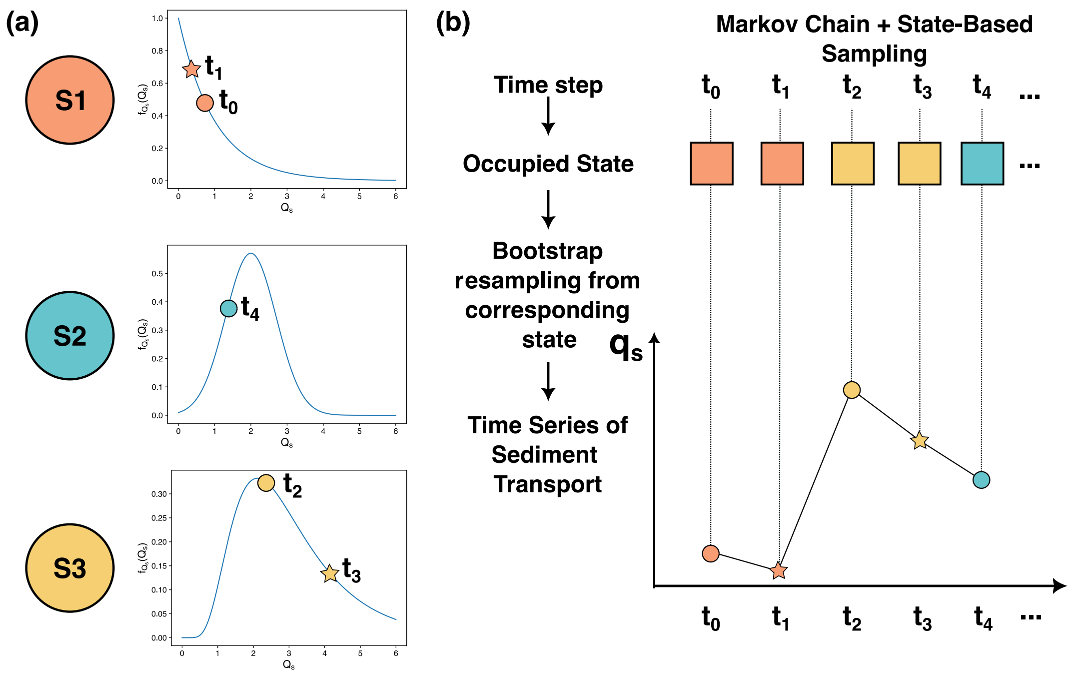

Figure 6. Illustration of state-conditioned sediment transport and resampling. (a) Empirical sediment-transport probability distributions associated with three states. (b) Example of state-based sampling applied to the first five elements of one realization of the state sequence, generating a synthetic sediment-transport time series.

4.2. Markov Model With Stream-Power–Based Parameterization

The preceding method necessitates direct transport measurements for each state, which may not always be feasible in practice. We now explore a more restrictive approach that infers transport statistics using morphological information and a scaling equation based on stream power. Our objective is to evaluate whether the statistical properties of sediment transport can be reconstructed from morphology alone, without directly using the empirical probability distributions of transport rates. To do so, we replace the state-conditioned resampling procedure with a parametric description of transport whose parameters are assumed to be functions of stream power.

The idea underpinning our approach builds on the scaling proposed by Bertoldi et al. (2009), who showed that the mean dimensionless bedload transport q^* in braided rivers follows an approximate power-law relation with dimensionless stream power ω^*. However, the experimental conditions of the present study fall outside the range of stream powers considered in that work. We therefore adopt their conceptual framework but estimate the scaling relation directly from the morphological states identified in the experiment.

To that end, for each state s we compute the stream power per unit width from planform-derived hydraulic quantities as

$$\omega_s = \frac{\rho_w g Q S}{b_s},$$

where Q is the water discharge, S the channel slope, b_s the effective flow width associated with state s, ρ_w the water density, and g the gravitational acceleration. The width b_s is a reach-scale effective wetted width, not a local width measured at the outlet. It was computed from the binary water masks as the wetted area of the imaged reach normalized by the reach length, and then averaged over all observations assigned to state s. Both stream power and bedload transport are then expressed in dimensionless form using the same scaling factor $\sqrt{g\,\Delta\, d_{50}^3}$, namely

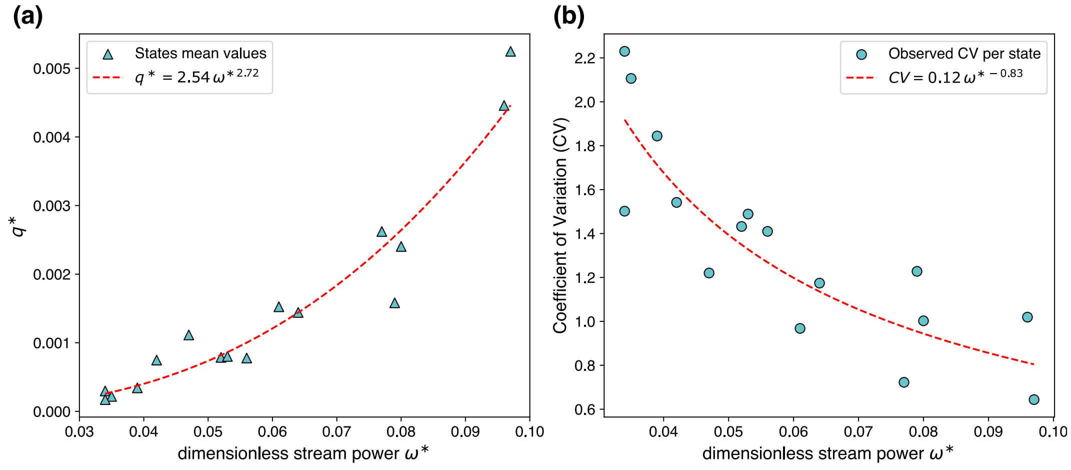

Figure 7. Stream-power-based parameterization of transport statistics. Left: fitted power-law relation between dimensionless stream power and dimensionless bedload transport across the morphological states. Right: fitted relation between stream power and coefficient of variation used to estimate within-state variability.

$$\omega_s^* = \frac{\omega_s}{\sqrt{g\,\Delta\,d_{50}^3}}, \qquad q_s^* = \frac{q_s}{b_s\sqrt{g\,\Delta\,d_{50}^3}},$$

where $\Delta = (\rho_s - \rho_w)/\rho_w$ is the relative submerged density and d_{50} is the median grain size.

For each state, we compute the mean dimensionless bedload transport $\mu_s = \overline{q_s^*}$ from the measurements collected while the system occupied that state, together with the coefficient of variation $\mathrm{CV}_s = \sigma_s/\mu_s$, where σ_s denotes the standard deviation of the transport rates. The relation between dimensionless stream power and mean transport across the 16 states is described by the power-law

$$q^* = a\,(\omega^*)^c, \tag{1}$$

where $c = 2.52$ is the exponent and $a = 2.54$ a multiplicative coefficient.

Figure 7a shows the resulting scaling between ω^* and q^* obtained from the state-level averages. We then repeat the procedure with the coefficient of variation and fit a power-law equation to the corresponding data (see Figure 7b), and find:

$$\mathrm{CV} = 0.12\,\omega^{*-0.83}. \tag{2}$$

Sediment transport within each state is represented by a Gamma distribution. This choice is motivated by the statistical properties of bedload transport, which is strictly positive and typically exhibits strongly right-skewed fluctuations with occasional high-transport events. The Gamma family provides a flexible parametric description for such variables while requiring only two parameters that can be directly related to the first two moments of the probability distribution.

In this formulation, transport in state s is drawn from the probability distribution

$$q_s^* \sim \mathrm{Gamma}\,(k_s, \theta_s),$$

where the shape parameter k_s and scale parameter θ_s are determined from the mean μ_s and variance σ_s^2 associated with that state:

$$k_s = \frac{\mu_s^2}{\sigma_s^2}, \qquad \theta_s = \frac{\sigma_s^2}{\mu_s}.$$

The mean μ_s is obtained from the fitted stream-power relation shown in Figure 7a, while the variance is estimated from the predicted coefficient of variation. In this way, both the mean and the variability of transport are derived from stream-power scaling, allowing the transport probability distribution for each state to be defined without directly using the empirical transport observations.

Once these parameters are defined for all states, sediment transport values can be generated for any simulated state sequence. The temporal structure of the time series is governed by the Markov transition matrix introduced in Section 3, while the magnitude and variability of transport are determined from the stream-power-based scaling relations.

Repeating this procedure for many realizations of the Markov chain produces an ensemble of synthetic sediment-transport time series generated from morphology and stream-power scaling alone.

4.3. Bootstrap Resampling Without Morphological States

One question that arises is whether we could achieve the same result (reproducing the variation in bedload transport rate q_s) by directly sampling the time series $q_s(t)$ without considering the morphological state of the bed. To that end, we use a technique called bootstrap resampling (Efron & Tibshirani, 1993), a standard resampling method, which involves repeatedly drawing values from the original data set with replacement. At each time step, a transport value is therefore sampled independently from the full set of measured q_s values.

The resulting sequence preserves the marginal probability distribution of sediment transport registered in the experiment. Because each draw is independent of the previous one, this procedure removes time correlations that arise from the ordered sequence of channel configurations. Periods of sustained high or low transport, if present in the observations, are not reproduced beyond what is implied by the overall probability distribution of q_s values.

For this reason, the bootstrap model represents a baseline in which sediment transport variability is treated as temporally unstructured. Comparing this reference with the state-based models introduced above allows us to assess the extent to which the dynamics of morphological states contribute to the statistical organization of sediment transport.

5. Evaluation of Statistical Performance

Each of the three models described above allows us to generate time series $q_s(t)$ of sediment transport rates. Due to the randomness in the time series, one result is not enough to compare how each model performs, and we therefore need another step, in which several realizations are generated using a Monte Carlo approach: for each model, we generate a large ensemble (1,000 realizations) of synthetic time series with the same length as for the experimental record.

We then evaluate model performance by comparing ensemble statistics with those derived from the experimental record. The quantities considered in this comparison include the mean and variance of sediment transport, return-period curves, and measures of temporal organization such as autocorrelation. This ensemble analysis provides insight into the degree to which the statistical properties of sediment transport are dependent on the dynamics of morphological states.

5.1. Mean and Variance of Sediment Transport

We begin by examining whether the three stochastic models reproduce the bulk statistical properties of the sediment-transport record. The mean transport rate represents the average sediment flux exported by the system, while the variance measures the magnitude of transport fluctuations and therefore provides a first indicator of variability. Because each model produces an ensemble of synthetic realizations, the probability distributions of the mean and variance across the Monte Carlo simulations can be compared directly with the experimental values. Figure 8 shows the probability distributions of ensemble means (top row) and variances (bottom row) obtained for the three models.

All three models reproduce the experimental mean transport with slight deviations. The bootstrap model yields an ensemble mean of $0.156\ \mathrm{g\,s^{-1}}$ with a relative error lower then 0.01%. The Markov model with empirical state-conditioned sampling provides a similarly accurate estimate, with a relative error of 0.17%. Even when the

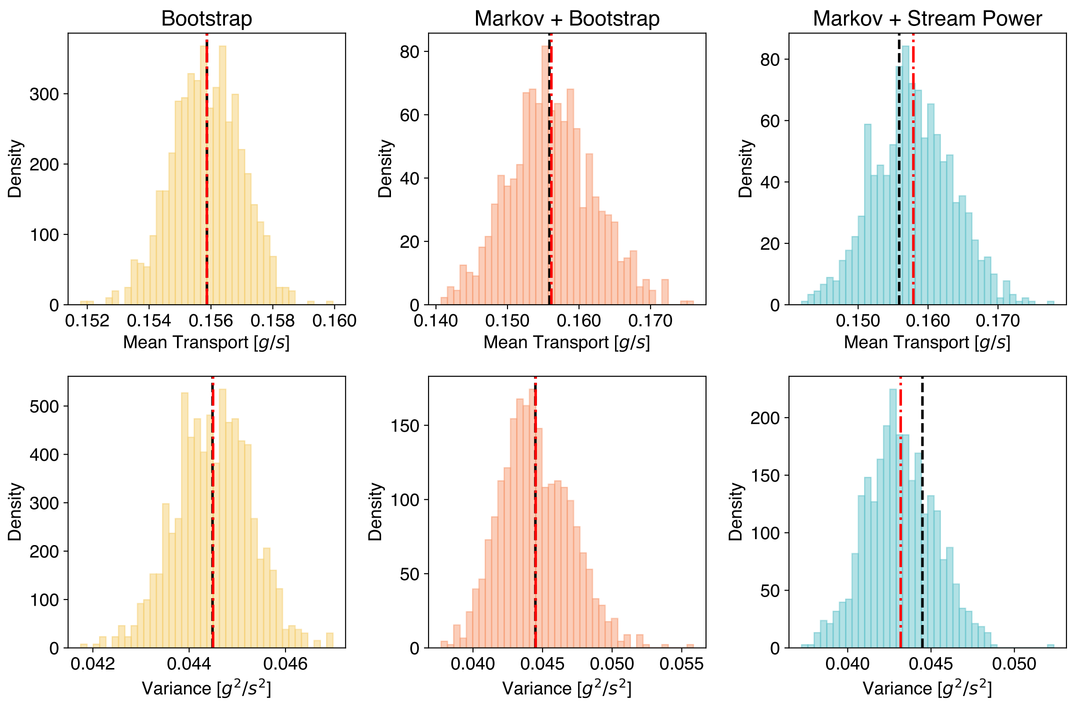

Figure 8. Distributions of mean sediment transport (top row) and variance (bottom row) obtained from Monte Carlo ensembles generated by the three stochastic models. Columns correspond to the bootstrap model, the Markov model with empirical state-conditioned sampling, and the Markov model with stream-power–based closure. Vertical dashed red lines indicate the experimental statistics, while black dashed lines show the ensemble means. All models reproduce the experimental mean and variance with small deviations, although the stream-power–based closure slightly underestimates the variance.

empirical transport probability distributions are replaced by the stream-power–based closure, the ensemble mean remains close to the experimental value, with a relative deviation of 1.30%. In the three cases, the experimental mean lies within the 90% confidence interval of the simulated ensembles.

Variance provides a more sensitive test of model performance because it reflects the magnitude of transport fluctuations. The bootstrap model reproduces the experimental variance almost exactly (with a relative error 0.03%), which is expected since the method resamples directly from the empirical transport record. Introducing state dynamics through the Markov model maintains this agreement, yielding a relative error of 0.04%. The stream-power–based model slightly underestimates the variance (relative error −2.93%), but the deviation remains small and the obtained value still falls within the ensemble confidence interval.

Overall, these results show that the three models reproduce the bulk magnitude and variability of sediment transport with high accuracy. Importantly, the close match found with the stream-power model shows that we can reproduce the main statistical features of the transport record from morphological states along with empirical scaling of q_s with ω^*, without needing to use the actual transport-rate probability distributions.

5.2. Extreme Transport Events and Periods of Return

We next examine whether the stochastic models reproduce the occurrence of extreme sediment-transport events. Such events play a pivotal role in cumulative sediment export and therefore provide a stringent test of model realism. To evaluate this aspect, we compare return-period curves derived from the Monte Carlo ensembles with those computed from the experimental record.

Figure 9 shows the relationship between sediment-transport magnitude and return period for the three models. The dashed black curve corresponds to the experimental record, while colored envelopes represent the 90% confidence interval (this interval is determined by keeping all the quantiles associated to empirical probabilities larger than 0.05 and lower than 0.95).

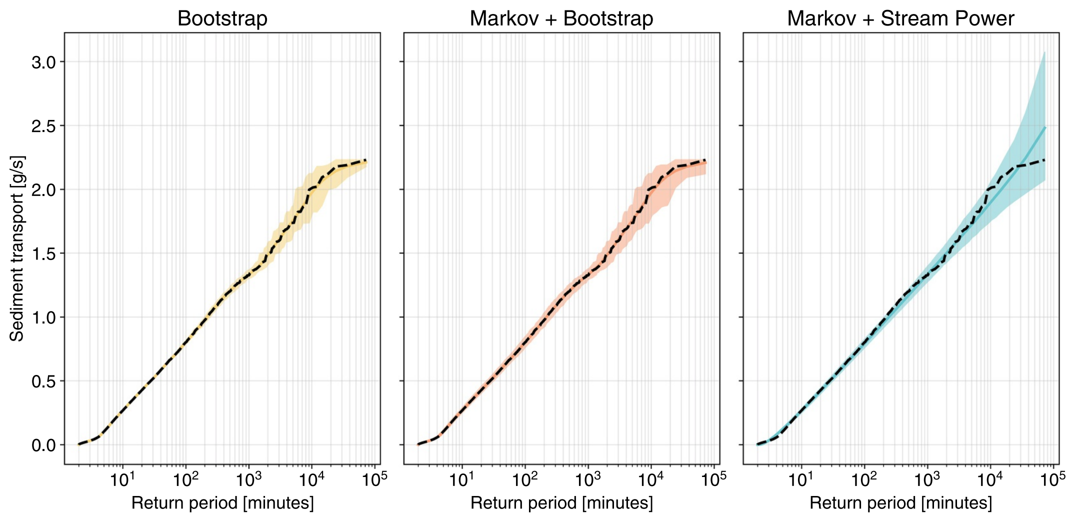

Figure 9. Return-period curves for sediment transport obtained from the three probabilistic models. The dashed black line corresponds to the experimental transport record, while colored envelopes represent the 90% confidence interval. The bootstrap and Markov models with empirical state-conditioned sampling reproduce the experimental return-period relationship with high accuracy. The stream-power model captures the overall trend of the return-period curve but produces a wider ensemble envelope at the highest return periods, indicating greater uncertainty and more variable extremes under the parametric state-level transport model.

The bootstrap model reproduces the experimental return-period curve almost exactly. The ensemble envelope captures the experimental behavior across the entire range of return periods, with a mean relative error of only 0.07%. This agreement is expected because the bootstrap model directly resamples from the empirical transport record and therefore preserves the tail behavior of the probability distribution.

The Markov model with empirical state-conditioned sampling shows a similarly strong performance. The simulated envelopes again encompass the experimental curve across the full range of return periods, with a mean relative error of 0.38%. This result indicates that combining state persistence with empirical state-level transport-rate probability distributions successfully reproduces both ordinary transport conditions and rare extreme events.

The stream-power model reproduces the overall shape of the return-period relationship. The simulated mean curve follows the experimental trend over most of the return-period range. At the highest return periods, however, the ensemble envelope widens substantially and the upper range of simulated outcomes exceeds the experimental curve. This widening reflects large variability in rare events across realizations, which is consistent with the use of Gamma distributions in the stream-power model. Although this model preserves the mean scaling between transport and stream power, it can generate more extreme values than the Markov model.

5.3. Temporal Properties of Transport Rate Time Series

Beyond reproducing the magnitude and variability of sediment transport, a realistic model must also capture how transport rate fluctuations vary over time. In braided rivers, transport events often cluster in time because morphological configurations persist for extended periods. To evaluate how well the three models reproduce this behavior, we compare the autocorrelation functions (ACF) and power spectral densities (PSD) derived from the simulated ensembles with those obtained from the experimental record.

The Wiener–Khinchin theorem states that for a stationary process, autocorrelation functions and power spectra give the same information but in different ways. The autocorrelation function measures how strongly a signal remains correlated with itself after a given time lag, thereby quantifying the persistence of fluctuations. In contrast, the power spectral density describes how the variance of a signal is distributed across frequencies and therefore reveals the dominant timescales of variability.

Figure 10 compares the autocorrelation function and power spectrum for each model: panel (a) shows the autocorrelation function as a function of time lag, while panel (b) presents the power spectral density of the transport signal. The experimental transport record exhibits strong persistence, with a rapid initial decay followed

10.1029/2026WR044293

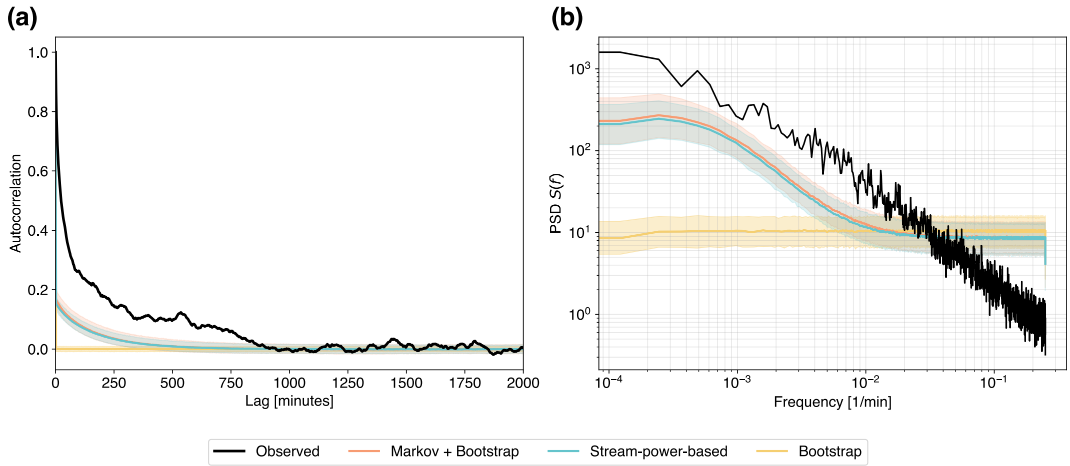

Figure 10. Temporal properties of sediment transport for the three stochastic models. Left: autocorrelation functions of the experimental record (black) and Monte Carlo ensembles. Right: power spectral densities. The bootstrap model produces nearly uncorrelated transport fluctuations, whereas the Markov-based models introduce persistence through the dynamics of morphological states. The Markovian and power-stream models capture the low-frequency variability of the signal, although they still underestimate the long correlation times of the experimental record.

by a long positive tail that extends over several hundred minutes. This structure indicates that transport fluctuations are organized across a wide range of time scales.

The bootstrap model fails to reproduce this temporal structure. Because transport values are sampled independently from the empirical probability distribution, the resulting time series behaves essentially as white noise. The autocorrelation decays almost immediately and the power spectrum remains nearly flat, lacking the pronounced low-frequency variability present in the experimental record.

Accounting for morphological state dynamics substantially improves the model performance by providing more realistic time variations in transport rate fluctuations. The Markov and stream-power generate persistent transport fluctuations and reproduce the initial decay of the autocorrelation function of the experimental record. In the spectral domain, the simulated signals also exhibit a clear negative slope, indicating variability across multiple time scales.

Despite this improvement, the models systematically underestimate the longest time scales present in the experimental record. The autocorrelation functions of the simulated series decay to zero faster than observed, and the power spectra contain less energy at the lowest frequencies. This discrepancy suggests that the persistence of morphological configurations in the experimental record exceeds what can be produced by a simple first-order Markov process, which assumes exponentially distributed residence times.

The comparison therefore indicates that morphological state dynamics capture an important part of the temporal organization of sediment transport, but that additional memory effects or longer residence-time statistics may be required to fully reproduce the long-term persistence observed in the experimental record.

6. Discussion

The results presented in Section 5 show that the statistical properties of sediment transport rates in the experimental record can be reproduced by a stochastic model that combines morphological state dynamics and state-level transport descriptions. Although all models reproduce the bulk magnitude of sediment transport, a large part of the temporal properties of the experimental record can be reproduced only when the persistence and transition features of morphological states are taken into account (Figures 8 and 10). These findings confirm that reach-scale sediment transport variability results from two distinct processes: the morphodynamic evolution of the channel through recurrent configurations and the transport behavior associated with each configuration.

In the following subsections, we discuss the implications of these results from three complementary perspectives: the role of morphological states in driving sediment transport variability, the interpretation of their dynamics within a Markovian model, and the predictive information contained in reach-scale morphology.

6.1. Morphological States Organize Sediment Transport Variability

A central result of this study is that much of the variability observed in the sediment-transport record is due to the succession of a finite set of recurrent morphological states (Figures 2 and 3). Although the inflow rates (water discharge and sediment feeding rate) remained constant during the experiment, the channel continuously reorganized through bar migration, channel splitting, and thread abandonment. These processes generated distinct planform configurations that persisted for extended periods before reorganizing into new ones. Because each configuration is associated with different riverbed shapes and transport capacity, the temporal sequence of states naturally produces fluctuations in sediment export.

From this perspective, variability in bedload transport rates is partially the consequence of regime switching between configurations with different transport capacities. Periods of sustained high or low flux occur because particular configurations persist in time before the system reorganizes into another state. The transport signal can therefore be interpreted as the combination of two sources of variability: fluctuations within a given morphological state and transitions between states with different transport characteristics (Figure 3). This decomposition provides the basis for the stochastic model developed in this study, in which the temporal evolution of morphology is represented as a Markov process governing transitions between recurrent channel configurations (Figure 5).

The contrast with the bootstrap model highlights the importance of this decomposition. Independent resampling preserves the probability distribution of transport magnitudes but removes the temporal organization associated with morphological persistence. As a result, the simulated series loses the clustering of transport events and collapses toward nearly uncorrelated fluctuations (Figure 10). This comparison indicates that sediment-transport variability cannot be explained solely by the probability distribution of transport magnitudes, but it arises from the time correlation imposed by morphological states.

6.2. Interpretation of the Markov Representation

The success of the state-based models suggests that the temporal evolution of reach-scale morphology can be effectively represented as a stochastic transition process between discrete configurations. In this representation, the probability of the next configuration depends only on the current morphological state. This assumption does not imply that morphodynamic processes are strictly memoryless. Instead, it reflects that the state variable captures much of the relevant information about the recent history of the system at the temporal resolution considered here. By describing the dynamics of these configurations through a transition matrix, the Markov model incorporates the persistence and switching of morphological states that ultimately organize the temporal structure of sediment transport.

Each morphological state corresponds to a class of planform configurations with similar channel-network organization. These configurations integrate the cumulative effects of hydraulic conditions, sediment transport, and bar dynamics over preceding time steps. The current state can therefore be viewed as a compact summary of the morphological conditions that influence the next reorganization of the channel.

Within this framework, the Markov model does not attempt to reproduce the exact sequence of morphological events observed in the experiment. Instead, it describes the statistical rules governing how configurations succeed one another and how long the system tends to remain in each one. Sampling from the transition matrix therefore generates an ensemble of statistically consistent morphological histories rather than a single deterministic trajectory. The experiment can then be interpreted as one realization drawn from a broader probability distribution of possible channel evolutions compatible with the transition structure.

The remaining discrepancies in correlation time suggest that some aspects of morphodynamic memory extend beyond the information contained in the current state (Figure 10). This result indicates that while the first-order Markov representation captures the dominant regime-switching dynamics of the channel, the longest time scales of sediment transport variability likely arise from slower morphodynamic adjustments that are not fully encoded in the instantaneous morphological configuration.

In a first-order Markov model, the probability of transitioning to the next state depends exclusively on the current state. In this sense, the system is memoryless, since earlier states have no direct influence once the present configuration is known. This assumption is analogous to ordinary differential equations, whose evolution is determined solely by the current state of the system. By contrast, higher-order Markov models introduce memory by allowing the transition probabilities to depend explicitly on the previous k states. This extension resembles integro-differential formulations, in which the present evolution reflects the cumulative influence of past states. Such models may provide a more faithful representation of gradual bar migration, sediment-storage cycles, and other slow morphodynamic adjustments that evolve over time scales longer than the observation interval. Likewise, semi-Markov representations offer an alternative means of accounting for memory by explicitly modeling residence-time probability distributions. Although these extensions are expected to provide a more realistic statistical description of channel persistence, they also entail a substantially greater computational cost due to the larger state space and increased complexity of the transition process.

6.3. Predictive Role of Morphology

An important implication of the present results is that a large fraction of the predictive information required to describe sediment transport at reach scale is already contained in the morphological state of the channel. This conclusion is supported by the performance of the stream-power model introduced in Section 4, in which empirical transport-rate probability distributions within each state are replaced by an empirical scaling between stream power and mean bedload transport combined with a parametric description of variability based on Gamma distributions. Despite this simplification, the resulting simulations reproduce the mean transport, its variance, and much of the temporal organization of the signal (Figures 8 and 10).

These results reveal a hierarchy of drivers of sediment transport. Stream power governs the magnitude of transport within a given configuration, while the transition dynamics of morphological states determine how these configurations alternate in time. The scaling Equations 1 and 2 therefore define the transport intensity associated with each state, whereas the stochastic evolution of states organizes these intensities into a temporally structured transport signal. From a predictive perspective, this structure suggests that sediment transport at reach scale may be approached by first describing the evolution of morphological states and then estimating the transport associated with each state.

Using empirical state-conditioned probability distributions in the Markovian model provides the most accurate representation of extreme events, whereas the stream-power model slightly smooths the upper tail of the probability distribution (Figure 9). This lower performance of the latter model reflects the loss of detailed information about within-state fluctuations rather than a failure of the underlying physical scaling. It may also reflect the simplified representation of active width: each morphological state is represented by a single reach-averaged effective width, which is appropriate for the mesoscale state description but cannot resolve local flow concentration, downstream convergence, or spatially heterogeneous sediment routing within the braided network.

More fundamentally, these results suggest that reach-scale morphology represents the crucial mesoscale variable that permits the linkage of hydraulic conditions to sediment transport. Each morphological state represents a particular organization of the channel network that controls how water discharge is partitioned among threads and how sediment pathways connect through the reach. Using morphological states gives a simple way to describe how energy and sediment spread in the braided system.

6.4. Limitations and Perspectives

The Markovian model picks up key features of the sediment-transport record, but it also shows some gaps and indicates where more work is needed.

The first limitation concerns the representation of morphological persistence. Although the Markov and power-stream models reproduce the bulk temporal properties of sediment transport rates, they underestimate the long correlation times observed in the experimental record. This discrepancy indicates that some aspects of morphodynamic memory are not fully represented by a first-order transition process. This limitation is consistent with the longer-term morphodynamic memory discussed in Section 6.2 and motivates future models that relax the first-order Markov assumption.

The second limitation arises from the assumption of steady state at large temporal and spatial scales. In the present experiment, discharge and sediment feed remained constant, allowing the transition probabilities to be treated as stationary. In real-world rivers, discharge variability may modify both the set of accessible morphological states and the transition probabilities between them.

The transition probabilities also characterize one constant-feed experiment that was approximately sediment-balanced over the analyzed interval. Different relationships between sediment supply and transport capacity may alter the frequency of channel avulsions and morphological state transitions, as observed in aggradational braided-river experiments (Ashworth et al., 2007). The inferred transition probabilities should therefore be interpreted as specific to this forcing regime rather than as universal equilibrium transition rates.

A related limitation concerns the scale represented by the sediment-transport measurement. In this experiment, sediment transport was measured only at the flume outlet and averaged over one-minute intervals. This signal should therefore be interpreted as the downstream sediment export statistically associated with the contemporaneous morphology of the bounded experimental reach, rather than as a direct instantaneous estimate of reach-averaged transport capacity. High-frequency sampling is nevertheless important in laboratory braided rivers: Vesipa et al. (2017) showed that sampling interval strongly affects estimates of morphodynamic activity and that survey intervals of approximately 4–8 min were needed to capture the relevant bed-elevation dynamics at the flume scale. Our one-minute sampling therefore resolves short-timescale morphological variability, but it does not remove the spatial limitation associated with measuring sediment transport only at the outlet. Spatially distributed transport measurements, tests using longer averaging windows, or explicit lagged comparisons between morphology and outlet flux would be needed to determine the spatial and temporal scale over which this state-transport relationship holds.

Comparisons with natural rivers would therefore require separating externally forced changes from the autogenic state transitions emphasized here. A first comparison could be made from repeated satellite, UAV, or time-lapse images by applying the same state-identification workflow to binary water masks and testing whether natural braided reaches also occupy a limited number of recurrent planform configurations (Middleton et al., 2019; Rowland et al., 2016; Schwenk et al., 2017). A second comparison would require independent estimates of sediment export or morphologic sediment budgets, because direct bedload measurements are rarely continuous at the reach scale in natural braided rivers. Existing field studies linking active width, planimetric change, and channel morphology to sediment transport suggest that such a comparison is feasible, but it would likely require conditioning transition probabilities on discharge stage and sediment-supply history (Ashmore et al., 2011; Bizzi et al., 2021).

Finally, the morphological states and transition matrix used here are inferred from a specific experimental configuration. Applying the model to other rivers requires identifying appropriate state definitions and estimating their transition structure from imagery or planform data. While the conceptual structure of the model is general, its parameters remain system-specific.

Despite these limitations, the results demonstrate that a fairly simple description based on stochastic transitions between morphological states provides a compact and physically interpretable model for describing sediment transport variability at reach scale.

7. Conclusions

Sediment transport in braided rivers is characterized by strong temporal variability and sudden bursts of sediment export. The results of the present study show that much of this variability can be interpreted through the alternance between a finite set of morphological configurations.

Using a long-duration (1200 hr) laboratory experiment conducted under steady state conditions (constant water inflow and sediment feeding rate), we have represented the evolution of reach-scale morphology as the succession of morphological states, the temporal evolution of which was modeled as a stochastic process. Sediment transport conditions are then assigned conditionally on the occupied morphological state using either empirical probability distributions of transport rate or Gamma distributions with parameters dependent on stream power.

The statistical properties of the experimental sediment-transport record are reproduced by the purely Markovian and power-stream models in which stochastic state dynamics are combined with state-conditioned transport. In particular, these two models capture the mean sediment flux, its variance, and the temporal clustering of transport events observed in the experimental record. In contrast, the third model we tested—a bootstrap model that resamples transport values independently from the empirical probability distribution—replicates the marginal probability distribution of transport magnitudes but fails to reproduce the temporal organization of the signal. This contrasted performance indicates that sediment-transport variability at reach scale is largely conditioned by the persistence and succession of morphological configurations rather than by the spread of transport magnitudes alone.

When looking at the predictions of temporal features of bedload transport rates, model comparison shows that the Markovian and power-stream models perform better than the bootstrap model mainly because they include morphological states. The first two models differ, however, slightly with regards to the prediction of extreme values. Indeed, the model predictions are quite similar regarding the average transport rate, its variance, and most time features of the signal, while most differences show up in the upper tail of the transport-rate probability distribution, where the power-stream model tends to smooth out rare high-transport events.

Our findings indicate that changes in sediment transport in braided rivers mostly happen due to random changes from one persistent morphology to another. Within our Markovian model, the morphological dynamics dictate the timing of transport events via the persistence and succession of channel configurations, while hydraulic conditions control how much sediment is transported for a given morphology. Morphological state is therefore the key driver linking the braided channel network and sediment transport capacity.

Our article revives the debate on local versus non-local control of bedload transport by water flow. For braided rivers, our experiments suggest that sediment transport depends to a significant degree on the riverbed configuration, meaning that transport is primarily governed by mesoscale processes rather than local processes.

Conflict of Interest

The authors declare no conflicts of interest relevant to this study.

Availability Statement

The image data set used in this study is publicly available through the Zenodo repository (Gotelli & Ancey, 2026) at https://doi.org/10.5281/zenodo.18554208.

Acknowledgments
We acknowledge the support of the Swiss National Science Foundation (Grant 200020_204108). Open access publishing facilitated by Ecole polytechnique federale de Lausanne, as part of the Wiley - Ecole polytechnique federale de Lausanne agreement via the Consortium Of Swiss Academic Libraries.

References

Aberle, J., Coleman, S. E., & Nikora, V. I. (2012). Bed load transport by bed form migration. *Acta Geophysica*, *60*(6), 1720–1743. https://doi.org/10.2478/s11600-012-0076-y

Ancey, C., Bohorquez, P., & Heyman, J. (2015). Stochastic interpretation of the advection diffusion equation and its relevance to bed load transport. *Journal of Geophysical Research: Earth Surface*, *120*(12), 2529–2551. https://doi.org/10.1002/2014jf003421

Ancey, C., Davison, A. C., Böhm, T., Jodeau, M., & Frey, P. (2008). Entrainment and motion of coarse particles in a shallow water stream down a steep slope. *Journal of Fluid Mechanics*, *595*, 83–114. https://doi.org/10.1017/s0022112007008774

Ancey, C., & Heyman, J. (2014). A microstructural approach to bed load transport: Mean behaviour and fluctuations of particle transport rates. *Journal of Fluid Mechanics*, *744*, 129–168. https://doi.org/10.1017/jfm.2014.74

Ashmore, P. (1988). Bed load transport in braided gravel-bed stream models. *Earth Surface Processes and Landforms*, *13*(8), 677–695. https://doi.org/10.1002/esp.3290130803

Ashmore, P. (1991). Channel morphology and bed load pulses in braided, gravel-bed streams. *Geografiska Annaler - Series A: Physical Geography*, *73*(1), 37–52. https://doi.org/10.1080/04353676.1991.11880331

Ashmore, P., Bertoldi, W., & Gardner, J. T. (2011). Active width of gravel-bed braided rivers. *Earth Surface Processes and Landforms*, *36*(11), 1510–1521. https://doi.org/10.1002/esp.2182

Ashworth, P. J., Best, J. L., & Jones, M. A. (2007). The relationship between channel avulsion, flow occupancy and aggradation in braided rivers: Insights from an experimental model. *Sedimentology*, *54*(3), 497–513. https://doi.org/10.1111/j.1365-3091.2006.00845.x

Ashworth, P., & Ferguson, R. (1986). Interrelationships of channel processes, changes and sediments in a proglacial braided river. *Geografiska Annaler - Series A: Physical Geography*, *68*(4), 361–371. https://doi.org/10.1080/04353676.1986.11880186

Bagnold, R. A. (1966). *An approach to the sediment transport problem from general physics (professional paper 422-I)*. United States Geological Survey.

Balmforth, N., & Provenzale, A. (2001). Patterns of dirt. In *Geomorphological fluid mechanics* (pp. 369–393). Springer.

Bertoldi, W., Ashmore, P., & Tubino, M. (2009). A method for estimating the mean bed load flux in braided rivers. *Geomorphology*, *103*(3), 330–340. https://doi.org/10.1016/j.geomorph.2008.06.014

Bizzi, S., Tangi, M., Schmitt, R. J., Pitlick, J., Piégay, H., & Castelletti, A. F. (2021). Sediment transport at the network scale and its link to channel morphology in the braided vjosa river system. *Earth Surface Processes and Landforms*, *46*(14), 2946–2962. https://doi.org/10.1002/esp.5225

Bohorquez, P., & Ancey, C. (2015). Stochastic-deterministic modeling of bed load transport in shallow water flow over erodible slope: Linear stability analysis and numerical simulation. *Advances in Water Resources*, *83*, 36–54. https://doi.org/10.1016/j.advwatres.2015.05.016

Bohorquez, P., Cañada-Pereira, P., Jimenez-Ruiz, P., & del Moral-Erencia, J. (2019). The fascination of a shallow-water theory for the formation of megaflood-scale dunes and antidunes. *Earth-Science Reviews*, *193*, 91–108. https://doi.org/10.1016/j.earscirev.2019.03.021

Bohorquez, P., Papa, D., & Ancey, C. (2025). Multi-train roll waves, antidunes and bars in inclined flumes. *Earth-Science Reviews*, *271*, 105308. https://doi.org/10.1016/j.earscirev.2025.105308

Charru, F., Mouilleron, H., & Eiff, O. (2004). Erosion and deposition of particles on a bed sheared by a viscous flow. *Journal of Fluid Mechanics*, *519*, 55–80. https://doi.org/10.1017/s0022112004001028

Dhont, B., & Ancey, C. (2018). Are bedload transport pulses in gravel bed rivers created by bar migration or sediment waves? *Geophysical Research Letters*, *45*(11), 5501–5508. https://doi.org/10.1029/2018gl077792

du Boys, P. (1879). Le rhône et les rivières à lit affouillable – étude du régime du rhône et de l'action exercée par les eaux sur un lit à fond de graviers indéfiniment affouillable. *Annales des Ponts et Chaussees*, *49*, 141–195.

Dubuisson, M.-P., & Jain, A. K. (1994). A modified Hausdorff distance for object matching. In *Proceedings of 12th international conference on pattern recognition* (Vol. 1, pp. 566–568). https://doi.org/10.1109/ICPR.1994.576361

Efron, B., & Tibshirani, R. J. (1993). *An introduction to the bootstrap*. Chapman and Hall/CRC.

Egozi, R., & Ashmore, P. (2008). Defining and measuring braiding intensity. *Earth Surface Processes and Landforms*, *33*(14), 2121–2138. https://doi.org/10.1002/esp.1658

Escauriaza, C., González, C., Williams, M. E., & Brevis, W. (2023). Models of bed-load transport across scales: Turbulence signature from grain motion to sediment flux. *Stochastic Environmental Research and Risk Assessment*, *37*(3), 1039–1052. https://doi.org/10.1007/s00477-022-02333-9

Falcini, F., & Garra, R. (2021). A nonlocal generalization of the exner law. *Journal of Hydrology*, *603*, 126947. https://doi.org/10.1016/j.jhydrol.2021.126947

Furbish, D. J., Fathel, S. L., & Schmeeckle, M. W. (2017). Particle motions and bedload theory: The entrainment forms of the flux and the exner equation. *Gravel-Bed Rivers: Processes and Disasters*, 97–120.

Furbish, D. J., Haff, P. K., Roseberry, J. C., & Schmeeckle, M. W. (2012). A probabilistic description of the bed load sediment flux: 1. theory. *Journal of Geophysical Research*, *117*(F3). https://doi.org/10.1029/2012jf002352

Gomez, B., Naff, R. L., & Hubbell, D. W. (1989). Temporal variations in bedload transport rates associated with the migration of bedforms. *Earth Surface Processes and Landforms*, *14*(2), 135–156. https://doi.org/10.1002/esp.3290140205

Gomez, B., & Soar, P. J. (2025). Utilitarian expressions for equilibrium bedload transport. *Hydrological Processes*, *39*(4), e70128. https://doi.org/10.1002/hyp.70128

Gotelli, C., & Ancey, C. (2026). Braided rivers as morphological states: A data-driven identification of recurrent planform configurations [Dataset]. *Zenodo*. https://doi.org/10.5281/zenodo.18554208

Guala, M., Singh, A., BadHeartBull, N., & Foufoula-Georgiou, E. (2014). Spectral description of migrating bed forms and sediment transport. *Journal of Geophysical Research: Earth Surface*, *119*(2), 123–137. https://doi.org/10.1002/2013jf002759

Kleinhans, M. (2004). Sorting in grain flows at the lee side of dunes. *Earth-Science Reviews*, *65*(1), 75–102. https://doi.org/10.1016/S0012-8252(03)00081-3

Li, Z., Peng, Z., Kiani-Oshtorjani, M., Liu, M., Zhang, F., Chen, Y., & Zhu, Y. (2024). A generalization of the exner law for sediment nonlocal transport at bedform scale. *Journal of Hydrology*, *645*, 132236. https://doi.org/10.1016/j.jhydrol.2024.132236

Limaye, A. B. (2020). How do braided rivers grow channel belts? *Journal of Geophysical Research: Earth Surface*, *125*(8), e2020JF005570. https://doi.org/10.1029/2020jf005570

McInnes, L., & Healy, J. (2017). Accelerated hierarchical density clustering. In *2017 IEEE international conference on data mining workshops (ICDMW)* (pp. 33–42). IEEE.

McInnes, L., Healy, J., & Melville, J. (2020). Umap: Uniform manifold approximation and projection for dimension reduction. Retrieved from https://arxiv.org/abs/1802.03426

Middleton, L., Ashmore, P., Leduc, P., & Sjogren, D. (2019). Rates of planimetric change in a proglacial gravel-bed braided river: Field measurement and physical modelling. *Earth Surface Processes and Landforms*, *44*(3), 752–765. https://doi.org/10.1002/esp.4528

Murray, A. B., Coco, G., & Goldstein, E. B. (2014). Cause and effect in geomorphic systems: Complex systems perspectives. *Geomorphology*, *214*, 1–9. https://doi.org/10.1016/j.geomorph.2014.03.001

Nikora, V. (1984). The structure of turbulent flow and statistical characterisation of dune-covered river beds (with examples of field studies in rivers turunchuk, rioni, and tsheniscali). [Unpublished Doctoral Dissertation].

Phillips, C. B., Hill, K. M., Paola, C., Singer, M. B., & Jerolmack, D. J. (2018). Effect of flood hydrograph duration, magnitude, and shape on bed load transport dynamics. *Geophysical Research Letters*, *45*(16), 8264–8271. https://doi.org/10.1029/2018gl078976

Phillips, J. D. (2003). Sources of nonlinearity and complexity in geomorphic systems. *Progress in Physical Geography*, *27*(1), 1–23. https://doi.org/10.1191/0309133303pp340ra

Redolfi, M., & Tubino, M. (2014). A diffusive 1d model for the evolution of a braided network subject to varying sediment supply. In *River flow* (Vol. 2014, pp. 1153–1161).

Rowland, J. C., Shelef, E., Pope, P. A., Muss, J., Gangodagamage, C., Brumby, S. P., & Wilson, C. J. (2016). A morphology independent methodology for quantifying planview river change and characteristics from remotely sensed imagery. *Remote Sensing of Environment*, *184*, 212–228. https://doi.org/10.1016/j.rse.2016.07.005

Schwenk, J., Khandelwal, A., Fratkin, M., Kumar, V., & Foufoula-Georgiou, E. (2017). High spatiotemporal resolution of river planform dynamics from Landsat: The RivMAP toolbox and results from the Ucayali River. *Earth and Space Science*, *4*(2), 46–75. https://doi.org/10.1002/2016EA000196

Simons, D. B., Richardson, E., & Nordin, C. (1965). Sedimentary structures generated by flow in alluvial channels.

Stecca, G., & Hicks, D. M. (2022). Numerical simulations of confined braided river morphodynamics: Display of deterministic chaos and characterization through turbulence theory. *Journal of Geophysical Research: Earth Surface*, *127*(3), e2021JF006409. https://doi.org/10.1029/2021jf006409

Sun, H., Chen, D., Zhang, Y., & Chen, L. (2015). Understanding partial bed-load transport: Experiments and stochastic model analysis. *Journal of Hydrology*, *521*, 196–204. https://doi.org/10.1016/j.jhydrol.2014.11.064

Vesipa, R., Camporeale, C., & Ridolfi, L. (2017). Effect of sampling time in the laboratory investigation of braided rivers. *Water Resources Research*, *53*(6), 5184–5197. https://doi.org/10.1002/2017wr020474

Wainwright, J., Parsons, A. J., Cooper, J. R., Gao, P., Gillies, J. A., Mao, L., et al. (2015). The concept of transport capacity in geomorphology. *Reviews of Geophysics*, *53*(4), 1155–1202. https://doi.org/10.1002/2014rg000474

Warburton, J., & Davies, T. (1994). Variability of bedload transport and channel morphology in a braided river hydraulic model. *Earth Surface Processes and Landforms*, *19*(5), 403–421. https://doi.org/10.1002/esp.3290190503